Defects induced by He+ irradiation in γ-Si3N4

Eduard Feldbach, Luc Museur, Veera Krasnenko, Andreas Zerr, Mamoru Kitaura, Andrei Kanaev

Defects induced by He^+ irradiation in γ-Si_3N_4

E. Feldbach,[a] L. Museur,[b] V. Krasnenko,[a] A. Zerr,[c] M. Kitaura,[d] A. Kanaev [c]*

[a] Institute of Physics, University of Tartu, 1 W. Ostwald str., 50411, Tartu, Estonia
[b] Laboratoire de Physique des Lasers, CNRS, Université Sorbonne Paris Nord, 93430 Villetaneuse, France
[c] Laboratoire des Sciences des Procédés et des Matériaux, CNRS, Université Sorbonne Paris Nord, 93430 Villetaneuse, France
[d] Faculty of Science, Yamagata University, 1-4-12 Kojirakawa, Yamagata 990-8560, Japan

Received XX Month XXXX; accepted XX Month XXXX

Abstract

Formation and evolution of defect levels in the electronic structure of silicon nitride with cubic spinel structure, γ-Si_3N_4, after the irradiation with He^+ ions was investigated using spectroscopic techniques. Strong changes of cathodoluminescence (CL), photoluminescence (PL), photoluminescence excitation (PLE) and Raman spectra were detected. In particular, excitonic PL was significantly inhibited and a new near-IR band appeared with the band gap excitation $h\nu \geq E_g$=5.05 eV. This was explained by an effective trapping of photoinduced electrons and holes by charged defects. The spectral shift of PL with the excitation photon energy indicated heterogeneous nature of the defect sites. The energetic position of near-IR and visible PL bands correlate, suggesting an interaction with the common cation defect to be an origin. The visible PL of exciton bound to a neutral defect $Si^{\times}$ was red shifted, which was attributed to the permutations between empty and occupied octahedral and tetrahedral sites, inherent to the spinel structure, after collisions with He^+ ions. The positively charged cation sites in the spinel structure are compensated by V_N''' anion vacancies. The local deformation of the spinel lattice affects PL intensity of the self-trapped exciton at 4.35 eV.

Keywords: Spinel Si_3N_4; He^+ irradiation; Cathodoluminescence; Photoluminescence; Structural defects

1. Introduction

Optical materials will play a substantial role in various diagnostic systems of future deuterium-tritium fusion reactors. For this reason, search and characterisation of those withstanding high intensity neutron fluxes must be pursued. Formation and nature of the radiation-induced lattice defects affecting functionality of the candidate materials for optical components in fusion reactors are under investigation in order to understand their radiation tolerance and find approaches of minimising the degradation rates. It is now widely recognized that the crystalline lattice of binary oxide spinels ($MgAl_2O_4$, etc.) possesses an elevated tolerance to the ionizing radiation [1, 2] due to an effective interstitial-vacancy recombination process and swapping of the cations between tetrahedral and octahedral sites, which take advantage of a huge number density of so-called structural vacancies in the crystal lattice: 7/8 of all available tetrahedral and 1/2 of octahedral sites. The energy cost for antisites formation in the spinel structure is much lower than that for all other elementary lattice defects [3] permitting to the cation sublattice easily accommodate the induced disorder.

The high-pressure (HP) binary nitrides with cubic spinel structure γ-M_3N_4 (M=Si, Ge, Sn) [4] could be alternative radiation tolerant materials, because the cation exchange in these materials does not result in the defect creation. Among the spinel nitride family, γ-Si_3N_4 [5] is the most prominent member, not only because it exhibits outstanding mechanical properties and exceptional thermal stability but also because it can be obtained as optical windows transparent in the VUV-vis-IR ranges of light [6]. The knowledge of the electronic band structure and structural defects is of importance in studies of its suitability for the application as radiation tolerant material.

The electronic band structure of the single-cation spinels nitrides has been predicted to be direct, with the E_g value between 3.45 eV and 4.97 eV in the case of γ-Si_3N_4 [7-10]. A slightly lower, by ~0.07 eV, indirect transitions than the direct transition of 5.16 eV have been recently calculated for this material [11]. Few calculations on the band structure distortion due to structural defects, vacancies or interstitials [12] and some frequent dopants [13] are also available. In contrast to the theoretical predictions, experimental data on the electronic structure of the spinel nitrides are rare. The first experimental study of the solid solutions γ-$(Si_{1-x}Ge_x)_3N_4$, where $0 \leq x \leq 1$, has been performed using soft x-ray spectroscopy [10] and later extended to γ-Sn_3N_4 [14]. Another detailed study of the defect and electronic band structure of γ-Si_3N_4 by time- and energy-resolved optical spectroscopy at LHe temperatures has been published only recently [15]. The band gap energy of E_g=5.05±0.05 eV and large exciton binding energy of D_e~0.65 eV have been reported, permitting to propose lighting applications of this material under severe external impact such as mechanical and/or radiation stress. The radiation tolerance and related modifications of the defect

* Corresponding author. Tel: +33-1-49403430; fax: +33-1-49403414;
E-mail: andrei.kanaev@lspm.cnrs.fr

and electronic band structure of γ-Si_3N_4 as well as other HP spinel nitrides have not been yet considered.

In this communication we report on the first investigation of the modification of photoluminescence (PL) properties and electronic transitions in γ-Si_3N_4 after irradiation with 150 keV He^+ ions (α-particles). The study was performed using UV-visible-near-IR time- and energy-resolved spectroscopy as most relevant and sensitive experimental method for the evaluation of changes of the electronic band and defect structures of solids.

2. Methods

The polycrystalline γ-Si_3N_4 sample of 3 mm diameter and 1 mm thickness was synthesized in a multi-anvil press at pressure of 15 GPa and temperature of 1700 °C by following the procedure described in Ref. [6]. The sample was partially sintered and translucent or transparent to the visible light after polishing. The prepared sample was mounted in a stainless still frame for PL measurements (Figure 1). One side of the sample was kept untreated and another was subjected to an ionizing radiation with He^+ ions of 150 keV energy and total dose of 10^{17} cm^{-2}. The irradiation was performed in the Accelerator Lab of Helsinki University.

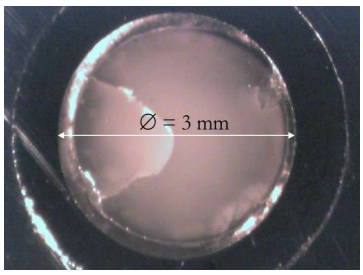

Fig. 1. View of γ-Si_3N_4 polycrystalline sample in a stainless steel ring mounting.

Both irradiated and pristine surfaces of γ-Si_3N_4 sample were structurally characterized using a set-up consisting of an IμS high Brilliance-Incoatec Microfocus Source Mo ELM33, delivering focused Mo $K\alpha_{1,2}$ radiation, and an Imaging Plate Detector with online readout system MAR345. The two-dimensional XRD patterns were collected in the grazing incidence geometry with the angle of ~7° and converted to the standard diffractograms $I(2\theta)$ using the Fit2D software [16]. This set-up permitted the detection of contaminating phases (e.g. β-Si_3N_4) in amounts as low as 0.5%, not accessible using standard diffractometers.

Prior to the optical measurements, the sample was removed from the stainless steel frame and fixed via silver glue on an aluminium support. Raman spectra were excited using the argon laser line λ_L=514 nm and collected with the Renishaw inVia micro-Raman installation; these measurements were performed with 100× objective at the normal incidence to the sample surface. The cathodoluminescence (CL) spectra of the spinel sample mounted on a close-cycle He cryostat were recorded at 5 K temperature using a laboratory installation [17]. The excitation was performed with an electron beam of 10 keV and 0.1 μA.

The photoluminescence (PL) experiments were carried out at the BL3B beamline [18] of the UVSOR synchrotron radiation facility with the excitation in VUV-UV-visible spectral range. The sample was mounted on the cold finger of a LHe flow type cryostat maintained during experiments at 9 K in the vacuum ~10^{-7} Pa. In order to evaluate structural damage induced by the irradiation, PL and PL excitation (PLE) spectra of the pristine and irradiated samples were collected and compared. The measured PLE spectra were corrected on the detector (AXUV100 photodiode) sensitivity and optical line transmission.

The energy of the tetrahedral and octahedral sites was evaluated from the theoretical calculations of the cationic (Si) and anionic (N) defect formation energies using general gradient approximation (GGA) [19] and 56-atoms 1x1x1 supercell, due to the low computational cost. These calculations were performed using the CASTEP module of the Materials Studio software [20].[#] Although, because of a small supercell the obtained values could not expected being accurate (especially for highly charged vacancies), they reflected general trends for the defects with different charge states, which has to be compared with the experiment. The screened hybrid functional approach of Heyd, Scuseria, and Ernzerhofnd with optimized screening parameters (HSE06) [21] for formation energy calculation on a primitive cell of Si_3N_4 with neutral Si tetrahedral monovacancy (provides more accurate result for Kohn-Sham energy levels) was performed as the benchmark [22] for the GGA calculations. Complementary, GGA calculations with 448 atoms 2x2x2 supercell of some selected defects were realized in order to check general trends obtained for the smaller 56-atoms supercell. To simulate charged defects, we have removed and added electrons to the defective cells/supercells. The formation energies of a neutral vacancy/point defect of Si_3N_4 were evaluated using the formalism described in Ref. [22]. The formation energy of a defect D in charge state q was defined as

$$H_{D,q} = E_{D,q} - E_{H,q} + \Sigma n_i \mu_{Di} \qquad (11)$$

where $E_{D,q}$ is total energy of the host-defect supercell and $E_{H,q}$ is total energy of the neutral host (if q=0) or charged host (if q≠0) of supercell without defects, μ_{Di} is the chemical potentials of the atoms removed (n_i=+1) or added (n_i=-1). Such approximation achieved good agreement with general trends of the charged defect formation energies by varying the supercell size [23].

3. Results and discussion

[#] The plane-wave basis energy cutoff was chosen to be 350 eV. The Monkhorst–Pack scheme k-points grid sampling was set at 6×6×6 for the Brillouin zone. The convergence parameters were set as follows: total energy tolerance $1.0\cdot10^{-5}$ eV/atom, maximum force tolerance 0.03 eV/Å, maximum stress 0.05 GPa and maximum displacement $1.0\cdot10^{-3}$ Å.

The XRD patterns of the pristine and He^+-irradiated sides of γ-Si_3N_4 crystal were identical (Fig. 2), showing no effect of the energetic ions on the crystalline structure and cubic cell parameters. In overall, the measured patterns confirmed an almost pure single phase sample with spinel structure, although a negligible admixture (up to 2 vol.%) of β-phase could be noticed. The relative amounts of β-Si_3N_4 and γ-Si_3N_4 phases did not change after irradiation.

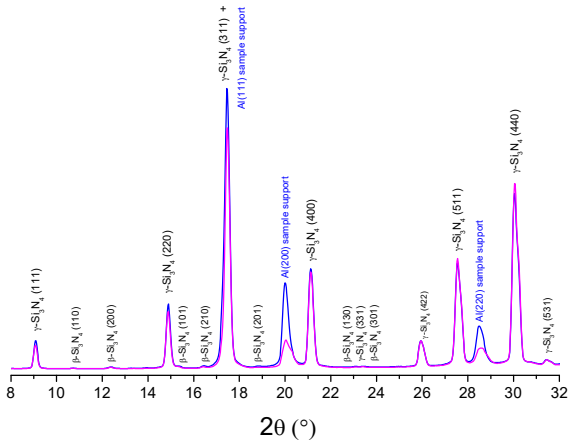

Fig. 2. X-ray diffraction patterns of γ-Si_3N_4 before (blue) and after (magenta) irradiation with He^+ ions. Intensities of Al-support peaks are different because of different illuminated areas after the sample rotation.

The examination by Raman spectroscopy (Fig. 3) confirmed the previous conclusion about the sample purity.

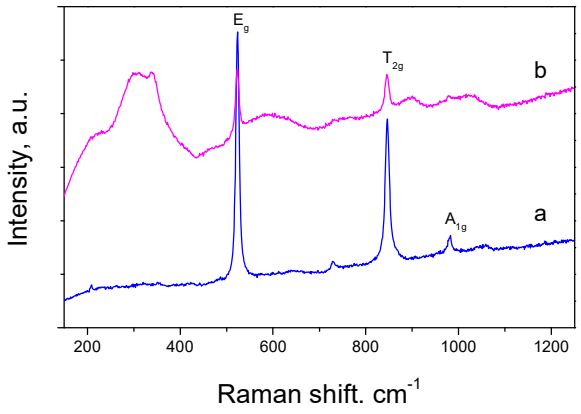

Fig. 3. Raman spectra of γ-Si_3N_4 before (a) and after (b) irradiation with He^+ ions.

The Raman spectra of pristine γ-Si_3N_4 (Fig. 3a) were dominated by two sharp intense bands at 524 and 847 cm^{-1}, in agreement with the earlier reports [24]. The higher frequency peak has been assigned to the T_{2g} asymmetric stretching mode of SiN_4 units and the lower frequency one to the E_g deformation vibration of SiN_4 groups (also SiN_6 stretching/bending); the somewhat weaker sharp band at 982 cm^{-1} has been assigned to the symmetric A_{1g} stretching vibration [25]. In contrast, Raman spectra of the irradiated sample (Fig. 3b) were strongly modified, indicating structural damage induced by H^+ ions. Indeed, sharp E_g, T_{2g} and A_{1g} modes weakened and broad bands appeared, which may be interpreted as a partial amorphisation of the material. However, Raman intensities cannot serve as a quantitative measure of the material phase composition. In fact, the absence of any significant amount of the amorphous material on the irradiated area is supported by XRD pattern in Fig. 2. The identical backgrounds of the XRD patterns before and after irradiation indicated that the amount of an amorphous material, if present at all, is minimal. The latter conclusion is further strengthened by the fact that the XRD measurements were performed in the grazing geometry which strongly enhances contribution of surface layers to the Bragg reflections. The additional broad features around 300-450, 550-650 and 900-1050 cm^{-1} have been earlier attributed to N^{3-} vacancies in the spinel structure, or to Si-N stretching/bending vibrations of SiN_3 units, associated with the formation of N^{3-} vacancies [25], which can be defined as V_N''' defects in Kröger–Vink notation [26]. The appearance of these negatively charged vacancies strongly indicates the creation of positively charged cation defects after the irradiation.

A wealth of information about cation defects can be obtained from the spectral analysis of the materials. The low-temperature CL spectra of the pristine and irradiated γ-Si_3N_4 samples are shown in Fig. 4. They contain two principal emission bands at 312 nm and 470 nm, which have been previously assigned to, respectively, self-trapped exciton and mixed contribution of exciton bound to neutral cation $X^*Si_{Si}^x$ and metastable paramagnetic nitrogen anion radical $N_N'^*$ [15]. A strong decrease of the CL intensity was observed after irradiation with He^+ ions, which is common to the spinel materials: the UV band was found totally suppressed while the visible band was attenuated by a factor of ~25.

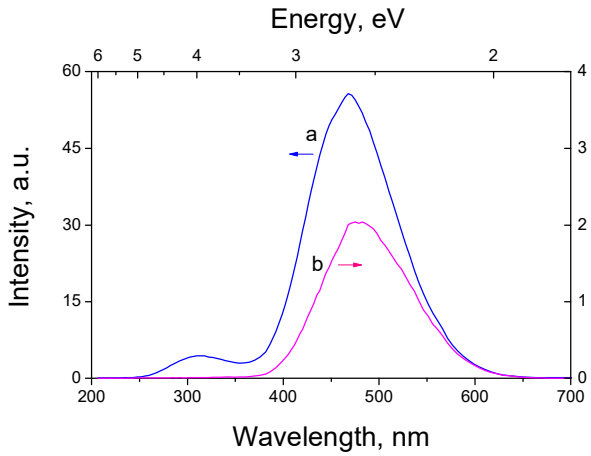

Fig. 4. CL spectra of γ-Si_3N_4 at T=5 K before (a) and after (b) irradiation with He^+ ions.

According to the previous analysis [15], longwave part of the visible band (λ_{PL}≈500 nm) is formed by the bound exciton $X^*Si_{Si}^x$ transitions and shortwave part (λ_{PL}≈450 nm) by the anion radical $N_N'^*$. The spectrum of the pristine sample (a) in Fig. 4 corresponds to a stronger contribution of the anion radicals, which can be formed after an electron

capture by neutral sites. The electron beam in CL measurements supplies electrons, hence favoring creation of such centers. The irradiation with positively charged ions can induce the suppression of such structural defect. Indeed, the spectrum in Fig. 4b indicates a significant attenuation of the shortwave part of this band compared to the longwave one, which, most probably, evidences this effect. The remaining luminescence belongs mostly to $X^{*}Si_{Si}^{x}$ centers. Resuming, we can conclude about the rapid quenching of excitons, which energy can be only partially transferred to the bound exciton luminescence.

The results of a SRIM (Stopping and Range of Ions in Matter) simulation indicated quite a high level of damage up to 5 dpa in the irradiated layer of $\delta \approx 0.6$ µm thickness (Fig. 5), which might signify the material amorphisation. Instead, a significant part of these displacements is expected to recombine, which results in a much smaller real concentration of various structural defects [27]. As CASINO calculations showed [28], the penetration depth of 10 keV electron beam matches the damaged layer, making CL a valuable source of information about its electronic structure. On the other hand, XRD patterns and Raman spectra also contain information from deep non-damaged layers ($d \geq 1$ µm) of the crystal. In particular, x-ray and Raman laser radiation in their respective experimental geometries could penetrate to the depth of about 3-10 µm and, consequently, result in ~80% of the signal from the pristine sample behind the damage layer. Even though these analyses cannot be considered as exclusively relevant to the damaged material, they quantitatively showed almost no long-range structural modification and a considerable short-range perturbation around the radiation induced defects.

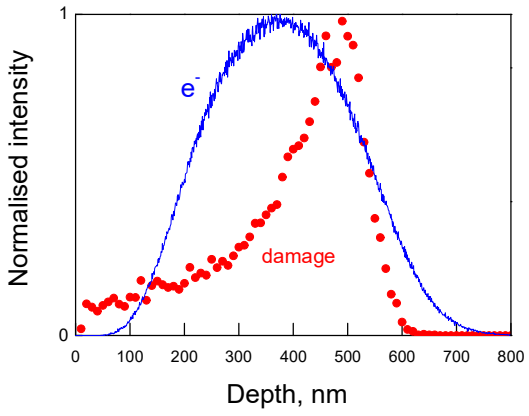

Fig. 5. Damage level induced by the He^{+} ions (maximum value ~4-5 dpa) and normalised number of CL electrons (10 keV) in γ-Si_3N_4 sample.

More detailed information about the material electronic structure provide excited state-selective PL and PLE measurements at cryogenic temperatures. Since characteristic absorption coefficients at the interband and excitonic transitions are $k > 10^4$ cm^{-1}, the penetration depth of the excitation photons in the UV spectral range $d < 1/k \sim 1$ µm corresponds to the penetration depth of He^{+} ions and therefore supplies state-selective information from the damaged material. The PL spectra of pristine and irradiated γ-Si_3N_4 sample sides are shown in Fig. 6. The emission of bound exciton $X^{*}Si_{Si}^{x}$ with the maximum at 495 nm (2.51 eV) dominates the spectra of the pristine sample (Fig. 6a). In contrast to CL, this spectrum seems to be free of N_N^{*} emission, in agreement with the e-beam induced centers formation. After the irradiation (Fig. 6b), its spectral maximum was red shifted to 525 nm (2.36 eV) by ΔE=-150 meV and a new near-IR band appeared with the maximum at 725 nm (1.71 eV). The near-IR band may be connected to that previously reported in pristine γ-Si_3N_4 sample at 860 nm (1.44 eV) tentatively assigned to Si_{Si}^{*} center excited by the exciton dissociation on Si_{Si}^{x} defect [15]. Obviously, any modification of the Si site would provoke simultaneous modifications of the trapped exciton and near-IR luminescence spectra. Conclusively, both the trapped exciton PL band shift and the new near-IR band appearance could indicate a modification of the cation sub-lattice. We notice that He bubbles, which might be produced in the spinel structure after the He^{+} ions irradiation would induce the spectral shift of the PL bands to higher energies, because of the dielectric relaxation of an emitting dipole in the vicinity of the excluded volume.

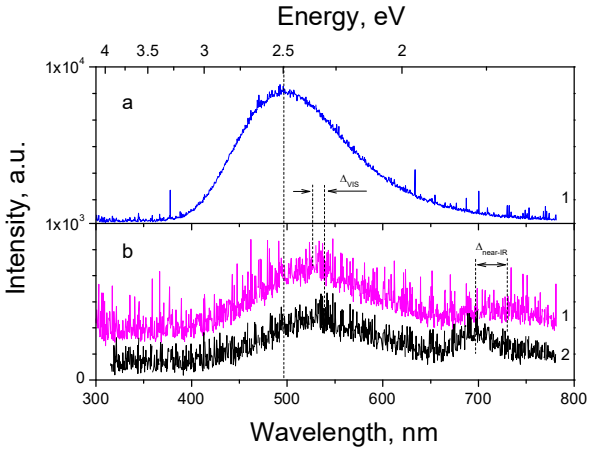

Fig. 6. PL spectra of γ-Si_3N_4 at T=9 K before (a) and after (b) irradiation with He^{+} ions, with excitation at 5.39 eV (230 nm) (1) and 6.89 eV (180 nm) (2); ΔE_1=150 meV and ΔE_2=210 meV. The energy shifts of the visible and near-IR bands are opposite: $\Delta_{near\text{-}IR} = -\Delta_{VIS}$ (where $\Delta_{VIS} \equiv \Delta E_2 - \Delta E_1 \approx$ 60 meV).

PLE spectra of the pristine and irradiated γ-Si_3N_4 sample sides are shown in Fig. 7. The pristine sample (Fig. 7a) is characterized by the interband transitions above E_g=5.05 eV and direct exciton transitions at about 4.35 eV (285 nm). In contrast, the interband transitions vanish after the irradiation (Fig. 7b) and a new band appeared at ~3.9 eV (320 nm). The corresponding absorption band due to these new PLE transitions is most probable reason for the strong screening and disappearance of the self-localized exciton PL at 4.0 eV (310 nm). We also notice that the red wing of the excitonic band at 4.5 eV in our non-irradiate sample extends to the lower energies and is stronger compared to that in a previously studied pristine γ-Si_3N_4 [15], as

respectively shown by solid and dotted lines in Fig. 7a. Moreover, the 3.9 eV photons excite the same PL band of the trapped exciton as via direct exciton transitions at 4.35 eV, as shown in pristine (Fig. 8a) and irradiated (Fig. 8b) samples, though the energetic position of the last one is red shifted by ΔE=74 meV. This refers to different environments of the emitting center.

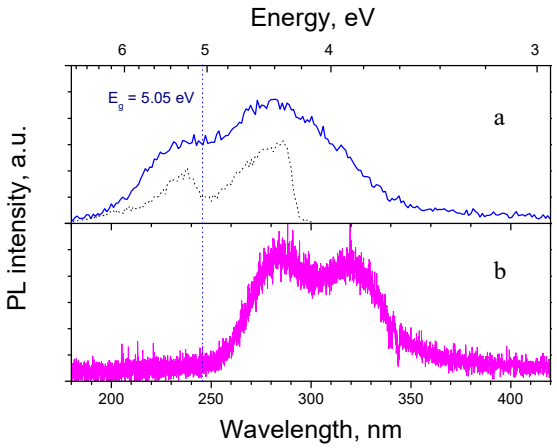

Fig. 7. PLE spectra at λ_{PL}=500 nm of γ-Si_3N_4 at T=9 K before (a) and after (b) irradiation with He^+ ions; dotted line shows PLE spectrum of the trapped exciton from Ref [15].

We observed from PLE spectra that, after the irradiation, the interband transitions (hν≥5.05 eV) were stronger attenuated than the excitonic transitions (4.35 eV), which is most probably connected to charged defects, which provoke an effective trapping and non-radiative recombination of the conduction band (CB) electrons and valence band (VB) holes. The strong inhibition of interband transitions is common for spinel materials [29-32]. In contrast, for non-charged particles, such as excitons, the radiative decay could be much more probable.

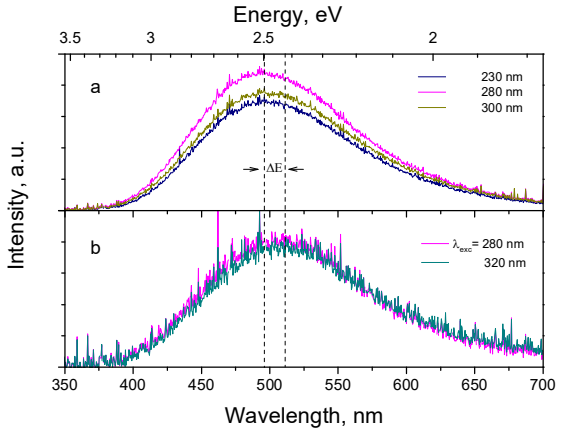

Fig. 8. PL spectra of γ-Si_3N_4 at T=9 K before (a) and after (b) irradiation with He^+ ions; excitation wavelengths are indicated; the spectral shift by ΔE=74 eV is indicated.

We adopted the following scheme of photoinduced processes in γ-Si_3N_4 explaining the observed PL bands:

$$X^* + Si^{\times} \longrightarrow X^*_{tr} - Si^{\times} \ (\lambda_{PL}=495\ \text{nm}) \quad (1)$$

$$X^* + Si^{\times} \longrightarrow h^{\bullet} + Si'^{*} \ (\lambda_{PL}=860\ \text{nm}) \quad (2)$$

$$Si_{Si} \xrightarrow{He^+} Si^+_{Si}, Si^+_{Vs} \quad (3)$$

$$Si_{Si} \xrightarrow{He^+} V^{\delta\prime}_{Si} + Si^{\delta\bullet}_{Vs} \quad (4)$$

$$N_N \xrightarrow{He^+} V^{\prime\prime\prime}_N + \tfrac{1}{2}N_2(g) \quad (5)$$

$$X^* + Si^{\delta\bullet}_{Vs} \longrightarrow X^* - Si^{\delta\bullet}_{Vs} \ (\lambda_{PL}=510\ \text{nm}) \quad (6)$$

$$e' + h^{\bullet} + Si^{\delta\bullet}_{Vs} \longrightarrow X^* - Si^{\delta\bullet}_{Vs} \ (\lambda_{PL}=530\ \text{nm}) \quad (7)$$

$$X^* + Si^{\delta\bullet}_{Vs} \rightarrow \times \ (near-IR) \quad (8)$$

$$e' + Si^{\delta\bullet}_{Vs} \longrightarrow Si^{(1-\delta)\prime *}_{V} \ (\lambda_{PL}=725\ \text{nm}) \quad (9)$$

where subscript *Vs* stands for structural vacancies inherent to the spinel structure. The processes (1)-(2) occur in the pristine sample and those (3)-(9) substitute (1)-(2) in the irradiated layer. The collisions of He^+ ion with Si_{Si} ionise (3) and displace cations to available structural vacancies $Si_{Vs}^{\delta\bullet}$ (4) by simultaneously producing compensating cation vacancies $V_{Si}^{\delta\prime}$. The processes (6), (7) and (9) replace (1) and (2) in the PL activation, involving respectively $Si_{Vs}^{\delta\bullet}$ and $Si_{Vs}^{(1-\delta)\prime *}$ defect states. According to our observations, in contrast to the pristine material, the exciton cannot excite the near-IR emission in the irradiated layer (8). Moreover, red shifts of the trapped exciton PL are different after the band gap (Fig. 6b) and direct exciton (Fig. 8b) excitations. The explanation of these results will be given below based on the previous assignment of PL and PLE bands [15] and correlations between their spectral shifts after the irradiation.

In fact, the formation of several cation defects Si_{Vs} can be assumed after the irradiation, which can be shared between the tetrahedral (1/8 occupied) and octahedral (1/2 occupied) voids as depicted in Fig. 9 below.

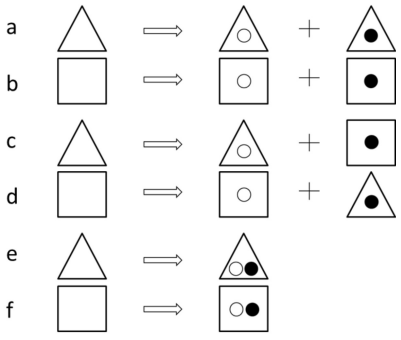

Fig. 9. Possible permutations of a cation between tetrahedral (Δ) and octahedral (□) voids resulting in formation of defects V_{Si} (○) and Si_{Vs} (●).

The energetic cost of permutations **a** and **d** (respectively **b** and **c**) may be different but they result in the similar cationic defect states in the tetrahedral ($Si_{Vt}^{\delta\bullet}$) and octahedral ($Si_{Vo}^{\delta\bullet}$) voids. These states are expected to be partially positively charged (0<δ<1) because of the local dielectric polarisation, which alters their energetic positions. In contrast, the permutations **e** and **f** within the same voids do not result in any appreciable energetic shift because of a short-range charge relaxation. The remaining

vacancies $V_{Si}^{\delta'}$ (partially negatively charged) weaken N_N bonds favouring the formation of compensating V_N''' defects. Because of a higher energy cost, the permutations **a-d** (Fig. 9) are expected to take place under the ionized irradiation, while those **e-f** may appear in the material during the synthesis and, therefore, depend on the synthesis conditions.

Our experimental observation of different spectral shifts of the trapped exciton PL after the band gap (7) and direct exciton (6) excitations suggests a significant energy gap between the cation defect states $Si_{Vt}^{\delta\bullet}$ and $Si_{Vo}^{\delta\bullet}$. Consequently, one of these states can receive a CB electron forming the near-IR emitting state (9); alternatively, this state can attract exciton leading to the visible PL (7). Another cation state can effectively trap an exciton leading to the visible PL (6), however cannot excite the near-IR emitting state (8). If this supposition is true, the energetic positions of the visible and near-IR emission bands would be expected to correlate. Indeed, two PL spectra in Fig. 6b obtained with the band gap excitation manifest opposite shifts of the visible and near-IR bands: $\Delta_{near\text{-}IR} = -\Delta_{VIS}$ (where $\Delta_{VIS} \equiv \Delta E_2 - \Delta E_1 \approx 60$ meV). We notice that (in contrast to the relative bands shifts in the irradiated spinel) the absolute energy shifts of the visible and near-IR bands between pristine and irradiated samples are much different because of different natures of the cation sites. In contrast to the neutral cation defect state $Si^{\times}$, the charged defect $Si_{Vs}^{\delta\bullet}$ suggests an additional energy decrease of the trapped exciton due to the charge-induced dipole interaction during its formation. On the other hand, the weak PL intensity after the band gap excitation ($h\nu \geq E_g$) could be explained by the dominant quenching channel relating the He^+ beam induced formation of charged cation defects (3):

$$e' + Si_{Si}^{+}, Si_{Vs}^{+} \rightarrow Si_{Si}^{\times}, Si_{Vs}^{\times} \qquad (10)$$

The results of the theoretical calculations of the formation energies of the cation and anion vacancies in γ-Si_3N_4 are shown in Fig. 10.

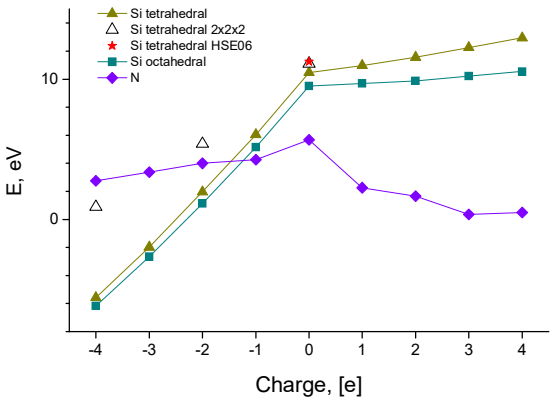

Fig. 10. Calculated trends in formation energy of charged cation (Si) and anoin (N) vacancies in the spinel structure of γ-Si_3N_4.

The formation energy of cation vacancies is lower than that of anion vacancy, which is a known feature of the spinel lattice caused by the presence of a huge amount of structural stoichiometric cation vacancies. The energy needed for swapping the cation position between octahedral and tetrahedral voids was estimated to be 0.95 eV for the neutral vacancies, which confirmed the tendency in $MgAl_2O_4$ spinel, where the formation energy for anti-sites defects is much smaller than any other point defect of the lattice [1, 33]. This low energy affords effective permutations of Si between the octahedral and tetrahedral positions during the irradiation by He^+ ions and, consequently, affects optical spectra of the spinel. The formation energy of Si defects (for the same charge) in the octahedral void are lower than that in the tetrahedral void, which can set the defect states ordering: $E(Si_{Vt}^{\delta\bullet}) > E(Si_{Vo}^{\delta\bullet})$. Although cation permutations within the same tetrahedral or octahedral voids, as depicted in Fig. 9 (e, f) might also result in some energy variation, they do not produce charged states; the same defect states are produced after permutations within a couple of voids t→o / t←o. Moreover, as our calculations showed, the new cation positions do not present local minima of energy and readily relax to the stable initial positions. Consequently, the permutations **a-d** (Fig. 9) between different voids could be expected to induce appreciable energy changes. In the opposite limit, we simulated cation permutations over a long distance after the irradiation.[#] For displacements, native 16*c* and 8*b* and perturbed 48*f*, 16*d* and 8*a* Wyckoff positions were chosen. For a convenience, the 56-atoms supercell was transformed (using VESTA program [34]) in a way to set the relevant Wyckoff positions in the cell center and the transformed cells were fully relaxed. Then, the 57th Si atom was placed in this Wyckoff position, the cell was positively charged +4 in order to compensate for extra electrons, and the atomic position were additionally relaxed in a fixed cell. The big 448-atoms supercells, having enough place to consider the displacement of atoms over relatively long distances ~1 nm, made from transformed and optimized 56-atoms supercells were also modelled, and the results on similar defects in the big and small supercells were compared. These calculations showed that the most energetically favourable position for permuted atom is 48*f* and least favourable is tetrahedral 8*a* with the energy difference of 7.25 eV. The energy difference between structures with permuted atom into 48*f* and 8*a* Wyckoff positions in 2x2x2 supercells were 7.62 and 9.23 eV, depending on which atom 8*b* or 16*c* was removed. The permutation from "native" 16*c* cell position to 8*a* was energetically more favourable than that from 8*b* to 8*a* with the energy difference of 1.61 eV. The energy difference between structures with permutated atom into 48*f* and 16*d* Wyckoff positions was 1.32 eV and 1 eV for 57-atoms and 448-atoms supercell, respectively.

The calculations showed that negative charging of Si_{Vs} defect moves its energetic position downwards, which suggests a higher energy of $Si_{Vs}^{(1-\delta)\prime *}$ defect level compared

[#] Due to a low computational cost, the plane-wave basis energy cutoff was chosen to be 250 eV. The Monkhorst–Pack scheme k-points grid sampling was set at 2×2×2 and 1x1x1 for the Brillouin zone respectively for small and big supercells. The convergence parameters were conserved.

with $Si_{Vs}'^{*}$. This could explain its weak interaction with exciton (Eq. (8)) and blue shift of the near-IR emission band (Eq. (9)). Based on the obtained results, an explanation of the defect related PL in the irradiated spinel crystal is the following.

(i) The lower energy octahedral $Si_{Vo}^{\delta\bullet}$ site can receive CB electron e' and VB hole $h^{\bullet}$, which annihilate forming trapped exciton X^{*}-$Si_{Vo}^{\delta\bullet}$. The free exciton X^{*} preferentially interacts with the energetically close-lying (quasi-resonant) defect state, which is tetrahedral $Si_{Vt}^{\delta\bullet}$, and annihilate forming trapped exciton X^{*}-$Si_{Vt}^{\delta\bullet}$.

(ii) The visible PL shifts to lower energies (compared to that in pristine spinel) because the charged cation site $Si_{Vt/Vo}^{\delta\bullet}$ induces an additional energy lowering due to a charge-dipole interaction with the exciton. The energetic position of the exciton bound to $Si_{Vo}^{\delta\bullet}$ is lower than that bound to $Si_{Vt}^{\delta\bullet}$.

(iii) The near-IR PL band is formed after the e' localisation on $Si_{Vo}^{\delta\bullet}$ and, therefore, its energetic position correlates with that of the trapped exciton at the same $Si_{Vo}^{\delta\bullet}$ site. The $Si_{Vt}^{(1-\delta)\prime*}$ state does not show up in PL since its energetic position is in the CB continuum of the spinel.

The low energy of cation permutations may result in a non-negligible, from spectroscopic point of view, number density of structural defects in the pristine sample. Indeed, the number density of such structural defects as large as 10^{20} cm^{-3} could be expected in the synthesised spinels [35], which may strongly affect PL spectra of even non-irradiated samples. Because of different intensities of the self-trapped exciton PL (4.35 eV) in different pristine spinel samples, as well as strong PL/PLE spectra modifications before and after irradiation, it can be assumed that natures of structural defects induced by the synthesis and irradiation are different, as respectively depicted by permutations **a**-**d** and **e**-**f** in Fig. 9. This confirms Fig. 7a, which compares PLE spectra of the bound exciton in two different pristine γ-Si_3N_4 samples: that from the present work (solid line) with non-appreciable PL of the self-trapped exciton absorbing at ~4 eV, that is in the range of the self-trapped exciton transitions, while that from Ref. [15] (dotted line) with a strong PL of the self-trapped exciton did not show any absorption in this spectral range. In particular, the cation permutations **e**-**f** in Fig. 9 within a tetrahedral and/or octahedral site may be a reason of the local lattice deformation, which induced absorption in the range of the self-trapped exciton radiative transitions, making this PL weaker or even cancelled. Future molecular dynamics calculations will shed light on the addressed issue.

6. Conclusion

Defects states created by He^{+} ions irradiation in a polycrystalline sample of γ-Si_3N_4 synthesised via high-pressure method were investigated. The defects analysis was based on previous assignment of the PL bands in the pristine material [15], correlation of their spectral positions and theoretical calculations of the formation energies of cation and anion vacancies in the octahedral and tetrahedral voids. We observed strong changes of cathodoluminescence, photoluminescence, photoluminescence excitation and Raman spectra after the irradiation, which can be interpreted as a partial disorder due to the formation of V_N''' anion vacancies and permutation of cations between filled Si_{Si} and empty V_{Vs} structural sites in the octahedral and tetrahedral voids.

The visible PL of the trapped exciton after the irradiation was significantly inhibited and red shifted and a new near-IR band appeared with the band gap excitation $h\nu \geq E_g$=5.05 eV, which is connected to the formation of the octahedral void defect $Si_{Vo}^{\delta\bullet}$. After the direct exciton excitation, the visible PL was explained by the formation of exciton bound to the tetrahedral void defect $Si_{Vt}^{\delta\bullet}$, which position is energetically higher than that of $Si_{Vo}^{\delta\bullet}$. The near-IR and visible PL bands are formed after the interaction of respectively e' and exciton with the common $Si_{Vo}^{\delta\bullet}$ site and their energetic positions correlate. In contrast, the tetrahedral site $Si_{Vt}^{\delta\bullet}$ does not show up in PL of the near-IR spectral region, because its energetic position is out of the spinel band gap. The local deformation of the spinel lattice may induce absorption in the spectral range of the self-trapped exciton transitions, which attenuates or even cancels the respective PL.

Acknowledgments

This work has been carried out within the framework of the EUROfusion Consortium and has received funding from the Euratom research and training programme 2014-2018 and 2019-2020 under grant agreement No 633053. The views and opinions expressed herein do not necessarily reflect those of the European Commission. The authors are indebted to Norimasa Nishiyama for providing the sample.

References

[1] K.E. Sickafus, L. Minervini, R.W. Grimes, J.A. Valdez, M. Ishimaru, F. Li, K.J. McClellan, T. Hartmann, Radiation tolerance of complex oxides, Science 289 (2000) 748-751.

[2] K.E. Sickafus, R.W. Grimes, J.A. Valdez, A. Cleave, M. Tang, M. Ishimaru, S.M. Corish, C.R. Stanek, B.P. Uberuaga, Radiation-induced amorphization resistance and radiation tolerance in structurally related oxides, Nat. Mater. 6 (2007) 217-23.

[3] C.A. Gilbert, R. Smith, S.D. Kenny, S.T. Murphy, R.W. Grimes, J.A. Ball, A theoretical study of intrinsic point defects and defect clusters in magnesium aluminate spinel, J. Phys. Condens. Matter. 21 (2009) 275406.

[4] A. Zerr, R. Riedel, T. Sekine, J. E. Lowther, W-Y. Ching, I. Tanaka, Recent advances in new hard high-pressure nitrides, Adv. Mater. 18 (2006) 2933-2948.

[5] A. Zerr, G. Miehe, G. Serghiou, M. Schwarz, E. Kroke, R. Riedel, H. Fueß, P. Kroll, R. Boehler, Synthesis of cubic silicon nitride, Nature 400 (1999) 340-342.

[6] S-D. Mo, L. Ouyang, W.Y. Ching, I. Tanaka, Y. Koyama, R. Riedel, Interesting physical properties of the new spinel phase of Si_3N_4 and C_3N_4, Phys. Rev. Lett. 83 (1999) 5046-5049.

[7] W.Y. Ching, S.D. Mo, L. Ouyang, P. Rulis, Theoretical prediction of the structure and properties of cubic spinel nitrides, J. Am. Ceram. Soc. 85 (2002) 75.

[8] I-H. Chu, A. Kozhevnikov, T.C. Schulthess, H-P. Cheng, All-electron GW quasiparticle band structures of group 14 nitride compounds, J. Chem. Phys. 141 (2014) 044709.

[9] T.D. Boyko, E. Bailey, A. Moewes, P.F. McMillan, Class of tunable wide band gap semiconductors γ-$(Ge_xSi_{1-x})_3N_4$, Phys. Rev. B 81 (2010) 155207.

[10] C.M. Caskey, J.A. Seabold, V. Stevanovic, W.A. Smith, D.S. Ginley, N.R. Neale, R.M. Richards, S. Lany, A. Zakutayev, Semiconducting properties of spinel tin nitride and other IV_3N_4 polymorphs, J. Mater. Chem. C 3 (2015) 1389-1396.

[11] I. Tanaka, K. Tatsumi, M. Nakano, H. Adachi, F. Oba, First-Principles Calculations of anion vacancies in oxides and nitrides, J. Am. Ceram. Soc. 85 (2002) 68-74.

[12] F. Oba, K. Tatsumi, I. Tanaka, H. Adachi, Effective doping in cubic Si_3N_4 and Ge_3N_4: A first-principles study, J. Am. Ceram. Soc. 85 (2002) 97-100.

[13] T.D. Boyko, A. Hunt, A. Zerr, A. Moewes, Electronic structure of spinel-type nitride compounds Si_3N_4, Ge_3N_4, and Sn_3N_4 with tunable band gaps: application to light emitting diodes, Phys. Rev. Lett. 111 (2013) 097402.

[14] L. Museur, A. Zerr, A. Kanaev, Photoluminescence and electronic transitions in cubic silicon nitride, Sci. Reports 6 (2016) 18523.

[15] N. Nishiyama, R. Ishikawa, H. Ohfuji, H. Marquardt, A. Kurnosov, T. Taniguchi, B-N. Kim, H. Yoshida, A. Masuno, J. Bednarcik, E. Kulik, Y. Ikuhara, F. Wakai, T. Irifune, Transparent polycrystalline cubic silicon nitride, Sci. Rep. 7 (2017) 44755.

[16] A.P. Hammersley, S.O. Svensson, M. Hanfland, A.N. Fitch, D. Hausermann, Two-dimensional detector software: From real detector to idealised image or two-theta scan, High Pressure Res. 14 (1996) 235-248.

[17] E. Feldbach, E. Tõldsepp, M. Kirm, A. Lushchik, K. Mizohata, J. Räisänen, Radiation resistance diagnostics of wide-gap optical materials, Opt. Mater. 55 (2016) 164-167.

[18] M. Kitaura, S. Tanaka, M. Itoh, A. Ohnishi, H. Kominami, K. Hara, Excitation process of Ce^{3+} and Eu^{2+} ions doped in $SrGa_2S_4$ crystals under the condition of multiplication of electronic excitations, J. Luminescence172 (2016) 243-248.

[19] A. Zerr, G. Miehe, G. Serghiou, M. Schwarz, E. Kroke, R. Riedel, H. Fuess, P. Kroll, R. Boehler, Synthesis of cubic silicon nitride, Nature 400 (1999) 340-342.

[20] E. Soignard, P.F. McMillan, Raman spectroscopy of γ-Si_3N_4 and γ-Ge_3N_4 nitride spinel phases formed at high pressure and high temperature: evidence for defect formation in nitride spinels, Chem. Mater. 16 (2004) 3533-3542.

[21] F.A. Kröger, H.J. Vink, Relations between the concentrations of imperfections in crystalline solids, Solid State Phys. 3 (1956) 307-435.

[22] K.E. Sickafus, A.C. Larson, N.Yu, M. Nastasi, G.W. Hollenberg, F.A. Garner, R.C. Bradt, Cation disorder in high dose, neutron-irradiated spinel, J. Nucl. Mater. 219 (1995) 128-134.

[23] D. Drouin, A.R. Couture, R. Gauvin, P. Hovington, P. Horny, H. Demers, CASINO V2.42 - A Fast and easy-to-use modelling tool for scanning electron microscopy and microanalysis users, Scanning 29 (2007) 92-101.

[24] V.T. Gritsyna, I.V. Afanasyev-Charkin, V.A. Kobyakov, Structure and electronic states of defects in spinel of different compositions $MgO{\cdot}nAl_2O_3$:Me, J. Am. Ceram. Soc. 82 (1999) 3365-3373.

[25] E. Feldbach, I. Kudryavtseva, K. Mizohata, G. Prieditis, J. Räisänen, E. Shablonin, A. Lushchik, Optical characteristics of virgin and proton-irradiated ceramics of magnesium aluminate spinel, Opt. Mat. 96 (2019) 109308.

[26] A. Lushchik, S. Dolgov, E. Feldbach, R. Pareja, A.I. Popov, E. Shablonin, V. Seeman, Creation and thermal annealing of structural defects in neutron-irradiated $MgAl_2O_4$ single crystals, Nucl. Inst. Meth. Phys. Res. B 435 (2018) 31-37.

[27] H. Spiridigliozzi, A. Pille, F. Schoenstein, L. Museur, E. Feldbach, H. Mändar, M. Kitaura, A. Kanaev, Photoluminescence of $MgAl_2O_4$ spinel ceramics doped with Ta_2O_5 and irradiated with He^+ ions, (2019) to be published.

[28] J.P. Perdew, K. Burke, M. Ernzerhof, Generalized Gradient Approximation Made Simple, Phys. Rev. Lett. 77 (1996) 3865.

[29] Accelrys Software Inc, Material Studio Release Notes, Release 6.1, Accelrys Software Inc, San Diego, 2012.

[30] A.V. Krukau, O.A. Vydrov, A.F. Izmaylov, G.E. Scuseria, "Influence of the exchange screening parameter on the performance of screened hybrid functionals", *J. Chem. Phys.*, **125**, 224106 (2006).

[31] Wu et al Scientific Reports (2018) 8:11408 | DOI:10.1038/s41598-018-29176-1.

[32] N.D.M. Hine, K. Frensch, W.M.C. Foulkes, M.W. Finnis, Supercell size scaling of density functional theory formation energies of charged defects, Phys. Rev. B 79 (2009) 024112.

[33] R. Smith, D. Bacorisen, B.P. Uberuaga, K.E. Sickafus, J.A. Ball, R.W. Grimes, Dynamical simulations of radiation damage in magnesium aluminate spinel $MgAl_2O_4$, J. Phys.: Condensed Matter 17 (2005) 875-892.

[34] K. Momma, F. Izumi, "VESTA 3 for three-dimensional visualization of crystal, volumetric and morphology data," J. Appl. Crystallogr., 44, 1272-1276 (2011).

[35] J.A. Ball, M. Pirzada, R.W. Grimes, M.O. Zacate, D.W. Price, B.P. Uberuaga, Predicting lattice parameter as a function of cation disorder in $MgAl_2O_4$ spinel, J. Phys.: Condens. Matter 17 (2005) 7621-7631.